

Favorable Collisional Demixing of Ash and Fuel in Magnetized Inertial Fusion

Ian E. Ochs

Department of Astrophysical Sciences, Princeton University, Princeton, New Jersey 08540, USA

Nathaniel J. Fisch

*Department of Astrophysical Sciences, Princeton University, Princeton, New Jersey 08540, USA and
Princeton Plasma Physics Laboratory, Princeton, New Jersey 08540, USA*

(Dated: September 13, 2022)

Magnetized inertial fusion experiments are approaching regimes where the radial transport is dominated by collisions between magnetized ions, providing an opportunity to exploit effects usually associated with steady-state magnetic fusion. In particular, the low-density hotspot characteristic of magnetized liner inertial fusion (MagLIF) results in diamagnetic and Nernst frictions which can demix thermalized ash from fuel, accelerating the fusion reaction. A simple diffusion model shows that increases in the fusion energy yield on the order of 10% are in fact possible.

PACS numbers:

Introduction: In inertial deuterium-tritium (DT) fusion, stratification of different ion species can significantly impact the fusion energy output. For instance, demixing of the fuel ions can reduce the fusion reaction rate [1–5]. Mixing of the fuel ions with ash and edge impurities can also quench the fusion reaction. Ideally, the ash and impurities should be separated from the fuel, while the fuel itself should remain as mixed as possible.

For magnetized inertial fusion (MIF) the ion stratification physics in the plasma can enter magnetized transport regimes more traditionally associated with steady-state magnetic fusion energy (sMFE) [6, 7]. In sMFE, the density is peaked on-axis, and diamagnetic frictions tend to drive high- Z_I impurities into the high-density core region on the ion-ion diffusion timescale [8, 9]. This deleterious effect can be partially mitigated by peaking the temperature on-axis, which tends to flush impurities outwards as a result of the Nernst thermal friction [10–13]. However, in MIF devices such as Magnetized Liner Inertial Fusion (MagLIF), the density is naturally peaked at the plasma edge, while the temperature is peaked on-axis in the fusion hotspot [14, 15]; thus both the density and temperature profiles are naturally arranged to transport ash outwards. Furthermore, the length of a MagLIF shot is comparable to the ion-ion diffusion timescale, and much longer than the ion-electron diffusion timescale on which the effects dissipate. Remarkably, the same transport effects that are deleterious in sMFE thus have the potential to significantly increase fusion gains in MIF.

We first identify, under the constraints of magnetized transport, the conditions under which demixing is likely to lead to significant gains in fusion energy. We then derive a one-dimensional model to quantify this effect, combining the classical transport equations with a well-established model describing the DT fusion reaction [16]. We show very significant gains, on the order of 10%, in fusion output. Although our model makes several simplifying assumptions, our results clearly reveal a new potential upside to magnetic inertial fusion.

Optimal distribution of ash: Magnetized transport

will rearrange the fuel and ash subject to the constraint of ambipolarity; i.e. without moving net charge. To appreciate the effect of this transport on the fusion rate, consider the optimal distribution of ash under this constraint, neglecting for simplicity heat transport and assuming that the thermal energy nT in the plasma is spatially constant.

Consider then two boxes, with a total number N reactants (charge e) and M ash particles (charge Ze) divided between them, so that box 1 contains a fraction β of the total reactants and a fraction γ of the total ash (Fig. 1). If the fusion reaction rate is N^2T^2 , then the total reaction rate over both boxes is:

$$\dot{E} = N^2 [\beta^2 T_1^2 + (1 - \beta)^2 T_2^2], \quad (1)$$

In ambipolar transport, fuel and ash can be exchanged between the two boxes, as long as the total charge in each box remains unchanged. Thus the fraction of total ion charge in box 1, Q_1 , remains unchanged, where

$$Q_1 \equiv \frac{N_1 + ZM_1}{N + ZM} = \frac{\beta N + \gamma ZM}{N + ZM}. \quad (2)$$

Our thermal energy assumption requires that such exchanges also leave the ion pressure P in each box unchanged, so that the temperature is determined from:

$$P \equiv T_1 (\beta N + \gamma M) = T_2 [(1 - \beta)N + (1 - \gamma)M] \quad (3)$$

When $Q_1 < 1/2$, box 1 has more energy per charge than box 2, and is thus analogous to the MagLIF hotspot.

Eqs. (1-2) fully define an optimization problem for the fusion power \dot{E} over γ , where the free parameters are Q_1 , P , and M/N . Although in general the solution is quite complicated, with maxima that can occur at the boundaries or interior of the physically relevant domain ($0 < \beta, \gamma < 1$), for $Z = 2$ and $Q_1 < \frac{1}{2}$, the maximum occurs at $\gamma \rightarrow 0$ for the vast majority of possible values for N , M , and Q_1 . In other words, reactivity is maximized when as much ash as possible is in the colder, higher-density box. Fortunately, this is exactly what classical magnetized transport effects tend to do.

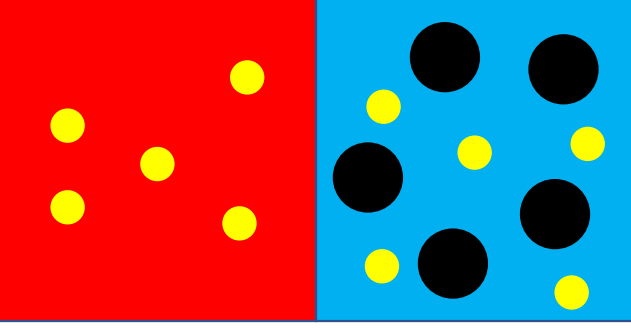


FIG. 1. Schematic of the optimization model. Here, there are $N = 10$ yellow fuel ions, and $M = 5$ black ash ions with $Z = 2$. For these parameters, box 1 (left) contains $Q_1 = 1/3$ of the total charge, while $T_1/T_2 = 2$. The optimal fusion power occurs when all the ash ions are in the colder box.

However, it should be noted that this conclusion is not necessarily valid when $\dot{E} \sim T^k$ for $k \neq 2$. It becomes optimal to place the ash in the hot box in the vicinity of $k = 1$ for $M \ll N$, and $k = 0$ for $M \gg N$. Thus, favorable effects from classical transport decrease at high temperature, where the fusion reaction scales less strongly with temperature.

Model: Given our understanding of the optimal distribution of ash, we now examine a physical model of transport and fusion. Denote the impurity by the subscript I , and the hydrogenic fuel ions by the subscript H . For implosion times long compared to an impurity-ion collision time τ_{IH} , and a compression velocity slow compared to the thermal velocity $\sqrt{T/m_i}$, the collisional transport motion due to ion-ion collisions is given by [7]:

$$\mathbf{v}_I^{(Tr)} = -\frac{T}{m_I \Omega_I^2 \tau_{IH}} \left\{ \frac{\nabla_{\perp} n_I}{n_I} - Z_I \frac{\nabla_{\perp} n_H}{n_H} + \left[1 + \left(\frac{3}{2} H_{HI} - 1 \right) Z_I \right] \frac{\nabla_{\perp} T}{T} \right\}, \quad (4)$$

where Ω_I is the impurity gyrofrequency, and

$$H_{HI} = \frac{1}{\sum_H n_H} \sum_H n_H \left(\frac{1 - Z_H m_H / Z_I m_I}{1 + m_H / m_I} \right) \quad (5)$$

is a numerical factor that determines the strength of the Nernst term (i.e. thermal friction), averaged over all hydrogenic species present [7]. For alpha ash interacting with an equal mix of deuterium and tritium, $H_{HI} = 3/7$.

To find the stationary state of the transport process, take $\mathbf{v}_I^{(Tr)} = 0$ and integrate Eq. (4) over space. The steady state radial distribution obeys:

$$n_I(r) \propto n_H(r)^{\frac{Z_I}{Z_H}} T(r)^{-\left(\frac{3}{2} H_{HI} - 1\right) \frac{Z_I}{Z_H} - 1}. \quad (6)$$

Taking the infinite-mass-ratio limit $H_{HI} \rightarrow 1$ of Eq. (6) yields the well-known classical impurity pinch result [8–

11]. For α ash, with $H_{HI} = 3/7$, Eq. (6) implies:

$$n_I(r)/n_H(r) \propto n_H(r) T(r)^{-2/7}. \quad (7)$$

Thus we find the fortuitous result that the ash will tend to be relatively concentrated in regions of high density and low temperature. The Nernst friction is critical to this result; if we took the Nernst-free limit $H_{HI} \rightarrow 0$, the temperature dependence would invert, and Eq. (7) would become $n_I/n_H \propto n_H T \approx P$; i.e. there would be no demixing in a constant-thermal-pressure plasma.

To quantify the effect of this demixing on the energy yield of the fusion reaction, we combine our transport model with a model for the fusion reaction:

$$\frac{\partial n_{\alpha}}{\partial t} \Big|_{\text{fus}} = \langle \sigma v \rangle (T) n_D n_T. \quad (8)$$

For $200 \text{ eV} < T < 100 \text{ keV}$, the reactivity $\langle \sigma v \rangle (T)$ can be analytically approximated to within 0.25% accuracy [16].

Consider the case of self-similar compression [17, 18], where the radial velocity due to compression is given by $v_r^{(C)}(r, t) = r \dot{R}(t)/R(t)$. This ensures that for a fluid element, $\tilde{r} \equiv r(t)/R(t)$ is constant in time. The function $R(t)$ will evolve on some characteristic stagnation timescale $\tau_s \sim \dot{R}(t)/R(t)$. The variables \tilde{r} and $\tilde{t} \equiv t/\tau_s$ thus represent the “natural” independent variables of the problem, with associated normalized dependent variables \tilde{n}_H , \tilde{n}_I , \tilde{T} , and \tilde{R} , related to the dimensional variables by

$$n_H(r, t) = \tilde{n}_H(\tilde{r}, \tilde{t}) n_{H0a} \tilde{R}(\tilde{t})^{-2} \quad (9)$$

$$n_I(r, t) = \tilde{n}_I(\tilde{r}, \tilde{t}) n_{I0a} \tilde{R}(\tilde{t})^{-2} \quad (10)$$

$$T(r, t) = \tilde{T}(\tilde{r}, \tilde{t}) T_{0a} \tilde{R}(\tilde{t})^{-2} \quad (11)$$

$$\tilde{R}(\tilde{t}) = R(t)/a. \quad (12)$$

The first two of these equations follow from the continuity equation, while the third is an ansatz which ensures thermal pressure balance during compression. We assume that the point of maximal compression occurs at $\tilde{t} = 0$, so that $\tilde{R}(\tilde{t} = 0) = 1$. We further assume that $\tilde{T} = 1$ and $\tilde{n}_H = 1$ at $(\tilde{t} = \tilde{t}_0, \tilde{r} = 1)$, where \tilde{t}_0 is the initial simulation timepoint, satisfying $\tilde{t}_0 \leq 0$. Thus n_{H0a} and T_{0a} represent the values of n_H and T at $(t = 0, r = a)$ in the absence of any diffusion or fusion, i.e. if the initial conditions were simply self-similarly compressed. Note that \tilde{n}_I is normalized to the value of \tilde{n}_H at $\tilde{r} = 1$, so that the relative densities of different species can be compared.

Our system will obey a continuity equation, incorporating the velocities due to transport (Eq. 4) and compression, as well as the source term from the fusion reaction (Eq. 8). Transforming the continuity equation to our nondimensionalized variables, we find:

$$\frac{\partial \tilde{n}_I}{\partial \tilde{t}} = \frac{1}{\tilde{r}} \frac{\partial}{\partial \tilde{r}} \left\{ \tilde{r} \tilde{n}_I D_0(\tilde{r}) \left[\frac{1}{\tilde{n}_I} \frac{\partial \tilde{n}_I}{\partial \tilde{r}} - Z_I \frac{1}{\tilde{n}_H} \frac{\partial \tilde{n}_H}{\partial \tilde{r}} + \left(1 + \left(\frac{3}{2} H_{HI} - 1 \right) Z_I \right) \frac{1}{\tilde{T}} \frac{\partial \tilde{T}}{\partial \tilde{r}} \right] \right\} + S \langle \sigma v \rangle (\tilde{T} T_{0a} \tilde{R}(\tilde{t})^{-2}) \tilde{n}_H^2, \quad (13)$$

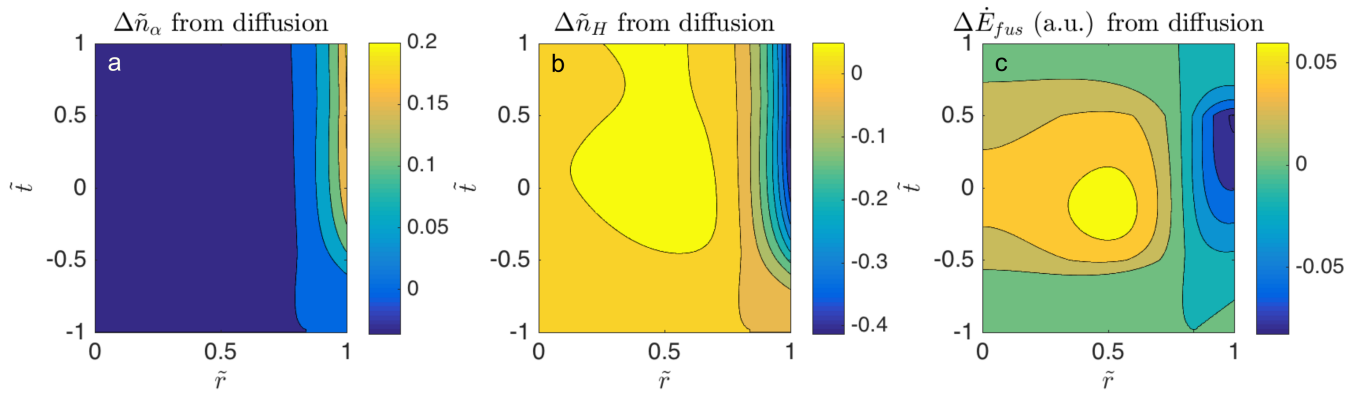


FIG. 2. Results from simulations of a stagnating plasma with a hot central core, both with and without diffusion. The figures show the difference in (a) α density, (b) fuel density, and (c) fusion reaction rate with diffusion vs. without diffusion, as a function of normalized radius and time. The magnetized diffusion results in more fuel in the hot central region and less in the periphery. This in turn increases the fusion reaction rate in the central region. Overall, the burn fraction is increased 10.8%.

where ambipolar transport, constant pressure, and magnetic flux compression imply that

$$\tilde{n}_H = \tilde{n}_{H0} + Z_I(\tilde{n}_{I0} - \tilde{n}_I) \quad (14)$$

$$\tilde{T} = (\tilde{n}_I + \tilde{n}_H)^{-1}, \quad (15)$$

$$D_{0a} = D_{0a} \tilde{n}_H \tilde{T}^{-1/2} \quad (16)$$

$$S = n_{H0a} \tau_s / 4. \quad (17)$$

The relevant dynamical timescales are determined by two dimensionless constants; the first is the number of diffusion times in a typical stagnation time τ_s :

$$D_{0a} = \left(\frac{\rho_{H0a}}{a} \right)^2 \frac{\tau_s}{\tau_{IH}} \quad (18)$$

$$D_{0a} = 0.7 n_{23} T_{10}^{-1/2} B_{10}^{-2} a_{100}^{-2} \tau_{s100}, \quad (19)$$

where $n_{23} = n_{0a}/(10^{23} \text{ cm}^{-3})$, $T_{10} = T_{0a}/(10 \text{ keV})$, $B_{10} = B/(10 \text{ kT})$, $a_{100} = a/(100 \text{ } \mu\text{m})$, and $\tau_{s100} = \tau_s/(100 \text{ ns})$. The second is the ratio between the burn time and implosion time:

$$S \langle \sigma v \rangle_{0a} = \frac{n_{H0a} \tau_s}{4} \langle \sigma v \rangle (T_{0a}) \quad (20)$$

$$\approx 0.3 n_{23} \tau_s T_{10}^2 \text{ for } 0.5 < T_{10} < 2. \quad (21)$$

There will be significant effects due to both diffusion and fusion over a stagnation time if $D_{0a} \gtrsim 1$ and $S \langle \sigma v \rangle_{0a} \lesssim 1$. Our magnetized transport assumption will be valid as long as the gyroradius is much smaller than the system size, i.e. $\rho_I/a \ll 1$, and the collision frequency is much smaller than the gyrofrequency, i.e.

$$\Omega_I \tau_{IH} = 7 n_{23}^{-1} B_{10} T_{10}^{3/2} \gg 1. \quad (22)$$

Implosion scenario: Eqs. (13-18) can easily be simulated in Matlab. To describe a MagLIF implosion, we take a form of $\tilde{R}(\tilde{t})$ suggestive of compression, followed by stagnation for $\Delta \tilde{t}_s = 1$, followed by expansion:

$$\tilde{R}(\tilde{t}) = \max \left[1, \exp \left(\tilde{t} - \frac{1}{2} \right) \right], \quad -\frac{\Delta \tilde{t}}{2} < \tilde{t} < \frac{\Delta \tilde{t}}{2}. \quad (23)$$

To simulate the low-density hotspot, we take:

$$\tilde{n}_{H0} = e^{\alpha(\tilde{r}^2 - 1)} \quad \tilde{T}_0 = e^{\alpha(1 - \tilde{r}^2)}. \quad (24)$$

Thus we can probe the effect of the profile steepness by changing α , with larger α corresponding to a steeper profile.

First, consider a MagLIF-like implosion scenario, with $B_0 = 12 \text{ kT}$, $T_0 = 6 \text{ keV}$, $n_0 = 5 \times 10^{22} \text{ cm}^{-3}$, $\tau_s = 500 \text{ ns}$, $a = 100 \text{ } \mu\text{m}$, and $\alpha = 1.5$. We take $\Delta \tilde{t} = 2$, but the results are generally insensitive to the simulation time since most fusion occurs over the stagnation. This is on the less dense and slower end for MagLIF implosion parameters, which we adopt to make sure that our orderings $\Omega_I \tau_{IH} = 0.12 \ll 1$ and $\rho_I/a = 0.0066 \ll 1$ remain valid; however, such effects are likely to persist into the mixed magnetization range $\Omega_I \tau_{IH} \lesssim 1$. For this choice of parameters, $D_{0a} = 1.5$ and $S \langle \sigma v \rangle_{0a} = 0.16$.

We carry out simulations both with and without the diffusion terms. As predicted by Eq. (7), the diffusion effects pull alpha ash out of the fusion hotspot to higher temperature (Fig. 2a). Because of the ambipolar transport constraint, this exclusion of ash results in an increased concentration of fuel in the hotspot (Fig. 2b). This in turn increases the fusion power in the hotspot, and decreases the fusion power at the edge (Fig. 2c).

Recalling our optimization problem, we see that the hot plasma center is effectively serving as the low- Q box. Because the fusion reaction scales as T^2 from $T = 5 - 20 \text{ keV}$, the optimal location for alpha ash is at the cold exterior of the plasma. Fortunately, magnetized transport effects move the ash towards this optimal location.

To quantify the effect on fusion yield, we can calculate the burnup fraction:

$$F_{burn} = \frac{\int_0^1 (\tilde{n}_{H0} - \tilde{n}_H) \tilde{r} d\tilde{r}}{\int_0^1 \tilde{n}_{H0} \tilde{r} d\tilde{r}}. \quad (25)$$

The impact of the diffusion terms can be captured by the fractional difference in burnup when diffusion is ignored

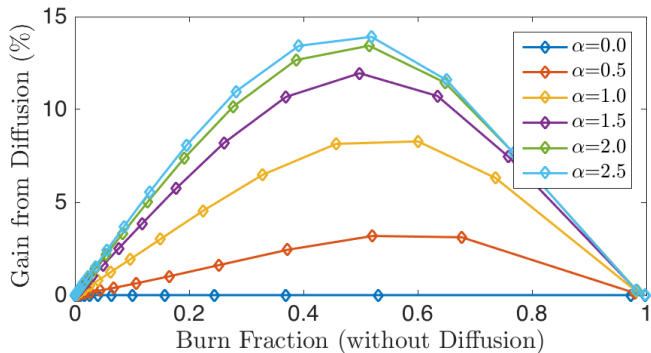


FIG. 3. Total diffusive gain G_D vs burn fraction F_{burn} (no diffusion) for several values of the profile steepness α (Eqs. 24). It is clear that higher gains occur at steeper density gradients as expected, with the gain saturating at around 13% at $\alpha = 2$. At this point, the hotspot temperature is 7.3 times hotter than the edge temperature.

or implemented, which we term the diffusive gain:

$$G_D \equiv \frac{F_{burn}(\text{diffusion}) - F_{burn}(\text{no diffusion})}{F_{burn}(\text{no diffusion})}. \quad (26)$$

In the present scenario, the burn fraction F_{burn} increases from 63.2% to 70.0% as a result of the demixing terms, representing a gain of $G_D = 10.8\%$ in the neutron yield.

Temperature distribution effects: The largest diffusive gains G_D occur when the burnup fraction is large enough that fuel depletion is a significant concern, but not so large that the marginal effect of diffusion is insignificant; i.e. G_D will be maximized in the regime around $F_{burn} \approx 50\%$, across a wide range of parameters (Fig. 3). Thus, to isolate the possible effect on G_D due to the different initial temperatures, we should compare parameter sets with comparable non-diffusive burn fractions $F_{burn}(\text{no diffusion})$.

To accomplish this level-playing-field comparison, we change the factor S in Eq. (13), without changing any of the other parameters in Eq. (13). Although such simulations do not necessarily represent physical parameter sets, they isolate the effect of an increased burn fraction fusion rate on the system, revealing the maximum potential gain from diffusion for a set edge temperature T_{0a} and profile steepness α . We then calculate this maximal gain G_D^* over S for a variety of parameter sets (T_{0a}, α) , which are shown in Fig. 4.

According to our optimization model, the demixing should be more important at lower edge temperature, where the fusion reactivity scales strongly with temperature. This is borne out in Fig. 4, where the maximum possible gains occur at the lowest edge temperature.

It is also intuitive that steeper profiles should produce greater diffusive gains, as seen in Fig. 4 at low temperatures. However, the simulations show that as the edge temperature increases, the steepness α at which G_D saturates decreases; in other words, there is less

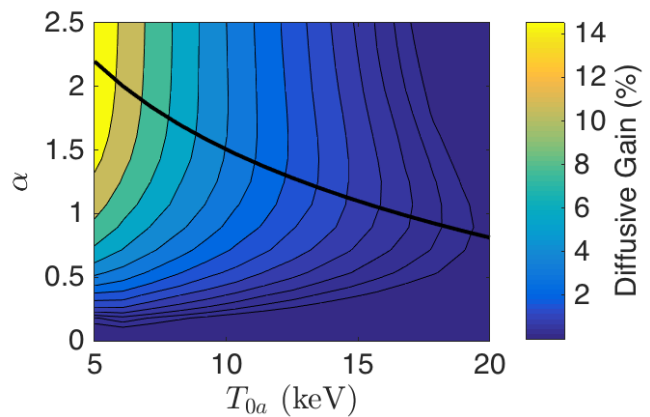


FIG. 4. Maximum diffusive gain G_D over burn rate S as a function of edge temperature T_{0a} and profile steepness α . All simulations have $D_{0a} = 1.5$. Diffusion has the greatest potential to increase the fusion yield when T_{0a} is low, and α is large. For a given T_{0a} , the diffusive gain significantly increases with profile steepness α until the central temperature reaches ~ 45 keV (black line), at which point it saturates. At higher D_{0a} , the potential gains grow larger by a factor of up to 30% [not shown].

benefit to a steeper profile at higher edge temperature. This saturation of G_D occurs around the point where the interior (hotspot) temperature becomes ~ 40 keV. Suggestively, 45 keV is roughly the temperature where the fusion reaction rate $\langle\sigma v\rangle(T)$ becomes flat with temperature.

Discussion: Remarkably, the diamagnetic and Nernst frictions can lead to favorable demixing of ash and fuel when the density and temperature profiles are oppositely peaked, leading to gains in fusion power on the order of 10%. Such increases in burnup could be instrumental in obtaining fusion breakeven, especially considering the large projected cost of magneto-inertial fusion reactors, which forces operation on the theoretical margin of ignition. The density and temperature gradients that optimized this favorable effect were also identified, and could be produced by laser-preheating the plasma core. These results depend on the plasma being in a regime where the fusion reactivity scales strongly with temperature, and the magnetized transport orderings are satisfied. The same physics leads to even more compelling demixing effects in a regime where impurities from the liner are also magnetized, in which case the impurities are likely to be expelled from the hotspot in the same manner. Although we assumed that $\Omega_I\tau_{IH} \ll 1$, such effects are likely to persist into the mixed magnetization regime $\Omega_I\tau_{IH} \lesssim 1$.

In arriving at these advantageous results, many simplifications were made. For instance, we ignored the possible effects of DT demixing on the fusion yield. Although such DT demixing should saturate at a much lower level than the α -fuel demixing, it might somewhat affect the

optimal profile steepness, since both fuel and ash demixing increase with profile steepness. In addition, we assumed constant magnetic field; however, in finite- β plasmas, the collisional interchange of ion species can involve an exchange of magnetic and thermal pressure, which could reduce the magnetic field in the hotspot.

We also neglected collisions with electrons. Although thermalized ash will collide primarily with ions, the slowing-down phase immediately after the ash birth will be dominated by collisions with electrons. This could affect the initial distribution of the thermalized ash, since asymmetries in the collisions with electrons could cause energetic alpha particles to be drawn to the colder, denser regions of the plasma even before they thermalize. However, such an effect would only add favorably to our results here, since it would lead to further favorable demixing of the ash. Other effects which could influence demixing include heat transport, plasma rotation [19], or turbulent transport from instabilities [20].

The promising phenomena predicted here ought to be

tested, which requires maintaining a low-collisionality plasma per Eq. (22). The fusion reactor parameter regime of MagLIF is characterized by magnetic fields around 1000 times larger and temperatures around 100 times higher than typical magneto-inertial experiments. Thus, in order to access the same magnetization regime, especially with a higher- Z_H bulk plasma, one would need densities around 6-7 orders of magnitude smaller than used here, i.e. in the range of $10^{15} - 10^{16} \text{ cm}^{-3}$. This is an unusual regime for current magneto-inertial experiments. However, given the highly encouraging predictions here for reactor parameters, such experiments seem worthwhile to attempt.

Acknowledgments: The authors thank Elijah Kolmes, Mikhail Mlodik, and Seth Davidovits for helpful discussions. This work was supported by NNSA 83228-10966 [Prime No. DOE (NNSA) DE-NA0003764], and by NSF PHY-1506122. One author (IEO) also acknowledges the support of the DOE Computational Science Graduate Fellowship (DOE grant number DE-FG02-97ER25308).

-
- [1] G. Kagan and X.-Z. Tang, *Physics of Plasmas* **19**, 082709 (2012).
- [2] C. Bellei, P. Amendt, S. Wilks, M. Haines, D. Casey, C. Li, R. Petrasso, and D. Welch, *Physics of Plasmas* **20**, 012701 (2013).
- [3] B. D. Keenan, A. N. Simakov, W. T. Taitano, and L. Chacón, *Physics of Plasmas* **25**, 032103 (2018).
- [4] E. Vold, G. Kagan, A. Simakov, K. Molvig, and L. Yin, *Plasma Physics and Controlled Fusion* **60**, 054010 (2018).
- [5] E. L. Vold, R. M. Rauenzahn, C. Aldrich, K. Molvig, A. N. Simakov, and B. M. Haines, *Physics of Plasmas* **24**, 042702 (2017).
- [6] S. Braginskii, *Reviews of plasma physics* **1**, 205 (1965).
- [7] F. L. Hinton, *Handbook of Plasma Physics* **1**, 147 (1983).
- [8] L. Spitzer Jr, *The Astrophysical Journal* **116**, 299 (1952).
- [9] J. Taylor, *Physics of Fluids* **4**, 1142 (1961).
- [10] S. Hirshman and D. Sigmar, *Nuclear Fusion* **21**, 1079 (1981).
- [11] P. Helander and D. J. Sigmar, *Collisional transport in magnetized plasmas*, Vol. 4 (Cambridge University Press, 2005).
- [12] M. Valisa, L. Carraro, I. Predebon, M. Puiatti, C. Angioni, I. Coffey, C. Giroud, L. L. Taroni, B. Alper, M. Baruzzo, *et al.*, *Nuclear Fusion* **51**, 033002 (2011).
- [13] E. Lerche, M. Goniche, P. Jacquet, D. Van Eester, V. Bobkov, L. Colas, C. Giroud, I. Monakhov, F. Casson, F. Rimini, *et al.*, *Nuclear Fusion* **56**, 036022 (2016).
- [14] S. Slutz, M. Herrmann, R. Vesey, A. Sefkow, D. Sinars, D. Rovang, K. Peterson, and M. Cuneo, *Physics of Plasmas* **17**, 056303 (2010).
- [15] S. A. Slutz and R. A. Vesey, *Physical review letters* **108**, 025003 (2012).
- [16] H.-S. Bosch and G. Hale, *Nuclear fusion* **32**, 611 (1992).
- [17] V. Velikovich, S. Gol'berg, M. Liberman, and F. Felber, *Sov. Phys. JETP* **61**, 261 (1985).
- [18] S. D. Ramsey, L. S. Brown, E. M. Nelson, and M. L. Alme, *A class of self-similar hydrodynamics test problems*, Tech. Rep. (Los Alamos National Laboratory (LANL), 2010).
- [19] E. Kolmes, I. Ochs, and N. Fisch, *Physics of Plasmas* **25**, 032508 (2018).
- [20] M. R. Weis, P. Zhang, Y. Y. Lau, I. M. Rittersdorf, J. C. Zier, R. M. Gilgenbach, M. H. Hess, and K. J. Peterson, *Physics of Plasmas* **21**, 122708 (2014), <https://doi.org/10.1063/1.4904210>.